

Wide Post-Mass Transfer White-Dwarf Binaries

Runqiu Ye

June, 2024

1 Introduction

Common envelope (CE) is the outcome of unstable mass transfer. During CE, both stars orbit inside an envelope and spiral inward. If the energy liberated in this process is enough to eject the CE, then the result of CE process is a close binary. If, on the contrary, the liberated energy is not enough to eject the envelope, then the result of the process is a merger. In observation results, a number of WD+MS binaries are wider than expected, and CE is expected to be the main channel to form these white dwarf binaries [Yamaguchi et al., 2024a, Yamaguchi et al., 2024b]. In the MESA model utilized by [Yamaguchi et al., 2024a, Yamaguchi et al., 2024b], wide post-CE WD+MS binaries can be formed in a certain range of initial separation with only gravitational and internal energy included in the calculation.

In this paper, we are going to explore the formation of these wide post-mass transfer WD+MS binaries with COSMIC model. We perform COSMIC simulation on both individual binary star systems and sampled population to explore the formation of WD+MS binaries under different conditions. In section 2, we are going to investigate formation of individual wide WD+MS binaries through CE for a variety of variables, including initial mass, initial separation, common envelope efficiency, and the energy budget of the CE. In section 3, we are going to explore the formation of individual wide WD+MS binaries through stable mass transfer. In section 4, we will research on how different COSMIC model affect simulation results of a sample population of binary star systems, and how the formation of post WD+MS binaries depends on various parameters.

2 Common Envelope

As argued in [Yamaguchi et al., 2024a, Yamaguchi et al., 2024b], unstable mass transfer is expect to be the main channel to form wide WD+MS binaries. In the MESA model, wide post-CE WD+MS binaries can be formed in certain range of initial separation. We hope to explore similar models in COSMIC.

In [Yamaguchi et al., 2024a], the lower limit of WD mass $M_{\text{WD,min}}$ in the observational sample is calculated to be $1.244M_{\odot} \sim 1.418M_{\odot}$. The corresponding mass of MS progenitor is expected to be in the range of $6 \sim 9M_{\odot}$, and the companion mass has median around $1M_{\odot}$. In [Yamaguchi et al., 2024b], the WD mass in the Gaia sample ranges from $0.5M_{\odot}$ to $0.8M_{\odot}$, which corresponds to progenitor mass of $1M_{\odot}$ to $3M_{\odot}$. The companions mass M_{\star} has a median of $0.85M_{\odot}$. Hence, we consider high mass systems using a $7M_{\odot} + 1M_{\odot}$ binary and low mass systems using a $1.5M_{\odot} + 0.85M_{\odot}$.

2.1 High mass systems ($7M_{\odot} + 1M_{\odot}$)

In [Yamaguchi et al., 2024a], the authors discussed currently observed wide post-mass transfer binary star systems. The MS progenitor of the WD star is expected to be in the range of $6 \sim 9M_{\odot}$. Therefore,

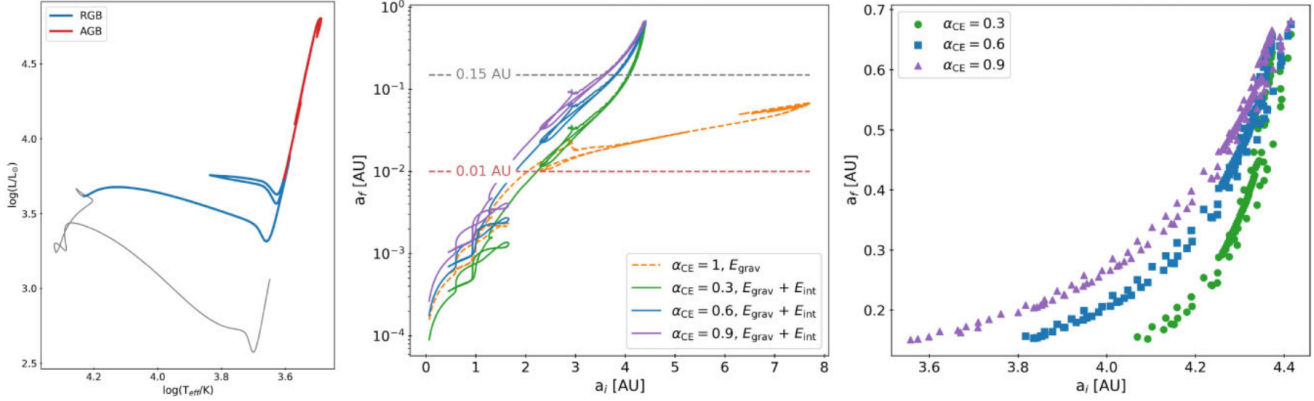


Figure 7. Left panel: HR diagram showing the evolution of a $7M_{\odot}$ star starting from pre-MS to the AGB. The blue sections indicate what we refer to as the RGB (but which also includes the SGB) and the red sections represent the AGB. Central panel: Plots of the final separation a_f (i.e. birth period at the end of CEE) over a range of initial separations a_i . a_i is taken to be the orbital semi-major axis when the giant (WD progenitor) fills its Roche lobe. We mark $a_f = 0.01$ au $\sim 2R_{\odot}$ (red dashed line) below which the MS star would not fit in the orbit and a PCEB cannot form. The orange dashed line is the case where only the gravitational binding energy is considered and $\alpha_{\text{CE}} = 1$. We see that in this case, no values of a_i result in $a_f > 0.15$ au (grey dashed line) which is approximately the minimum separation of our objects. The other three lines are the cases where all of the internal energy is added to the binding energy for $\alpha_{\text{CE}} = 0.3, 0.6$, and 0.9 . We see that these lines lie above the dashed line for some range of a_i . Right panel: Zoom in on the region where $a_f > 0.15$ au. We see that overall, $a_i \sim 3.5\text{--}4.4$ au can result in the wide orbital separations of our systems.

Figure 1: Results of how final separation a_f after common envelope depends on initial separation a_i for different common envelope efficiencies and energy budgets in [Yamaguchi et al., 2024a].

MESA model of a $7M_{\odot}$ star is run, and the evolution up to AGB is followed. After that, the change of separation through common envelope is calculated with

$$E_{\text{bind}} = \alpha_{\text{CE}} \left(-\frac{GM_{\text{WD}}M_{\star}}{2a_f} + \frac{GM_iM_{\star}}{2a_i} \right).$$

The binding energy on LHS is calculated as

$$E_{\text{bind}} = E_{\text{grav}} + E_{\text{int}} = \int_{M_{\text{core}}}^{M_{\text{tot}}} -\frac{Gm}{r(m)} + U(m)dm$$

or

$$E_{\text{bind}} = E_{\text{grav}} + \alpha_{\text{th}}E_{\text{th}} + \alpha_{\text{rec}}E_{\text{rec}}.$$

The results is presented in Figure 1, and we want to compare how this energy budget matches with the binding energy in COSMIC. Usually, the binding energy of the common envelope can be included in a structure parameter λ such that

$$E_{\text{bind}} = \frac{GM_iM_{\text{env}}}{\lambda R_i}. \quad (1)$$

This λ is represented in COSMIC as the `lambdaf` flag in `BSEDict`. Hence, we want to calculate the effective λ in COSMIC that matches these binding energy models in MESA.

2.1.1 Methods and results

To compare model in COSMIC with model in MESA, we run COSMIC binary simulation of a $7M_{\odot}+1M_{\odot}$ system. We want to see how the final separation a_f depends on the initial separation a_i and the common envelope parameter λ . Hence, we vary the initial separation in range $2 \sim 8$ au and the common envelope

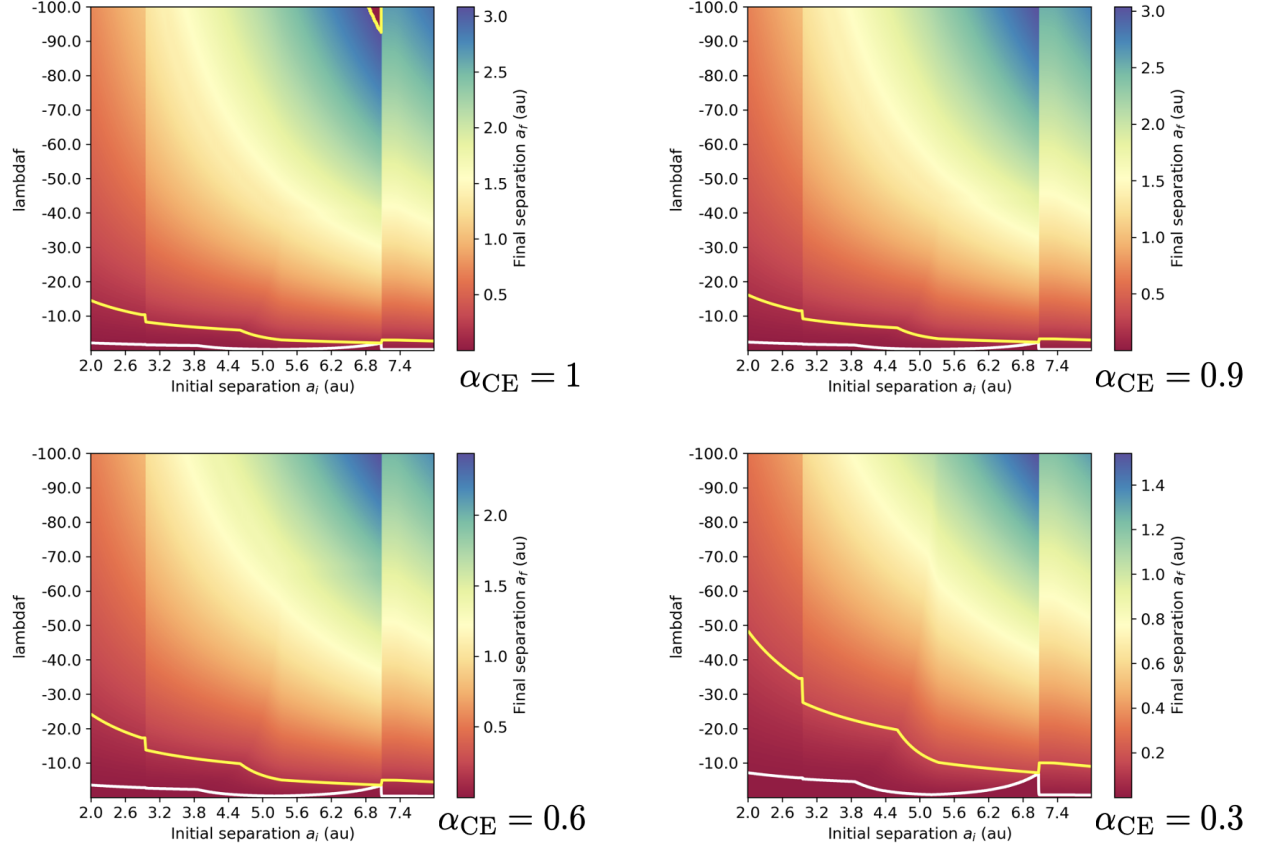


Figure 2: COSMIC results of how final separation a_f depends on initial separation a_i and common envelope flag "lambda_daf" for different common envelope efficiencies α_{CE} , where the black and red contour corresponds to 0.01 au and 0.15 au as in Figure 1 respectively. Outside the black contour no desired system forms.

flag `lambda_daf` in range $0 \sim -100$, which corresponds to $0 \sim 100$ for λ . Also, we run these parameters with four different common envelope efficiencies — $\alpha_{CE} = 1$, $\alpha_{CE} = 0.9$, $\alpha_{CE} = 0.6$, and $\alpha_{CE} = 0.3$.

After simulation is finished, we select the timestep that the system finished common envelope for the first time (`evol_type = 8`). At this moment, if the system is a WD+MS system, we record their separation as the final separation a_f . Otherwise, we set $a_f = 0$ and consider this initial condition unable to produce a WD+MS system.

We write the resulting final separations into `csv` files and create four heat maps for the four different common envelope efficiencies, as shown in Figure 2.

2.1.2 Discussions

Taking a closer look as the heatmap in Figure 2, we notice a few interesting points.

First of all, as α_{CE} decreases, the final separation decreases in general. This is expected and can be clearly derived from the formula. Qualitatively, more energy from the orbit is needed to eject the envelope for low α_{CE} , so the resulting a_f is smaller.

In addition, it is worth noting that most of these systems experience two mass transfer phases in COSMIC before reaching WD+MS. That is, two common envelope phases take places, between which there's a period of time. For some cases `kstar_1` changes during this period.

Also notice that the final separation a_f jumps obviously at about 2.9 au, and 7.1 au, which can

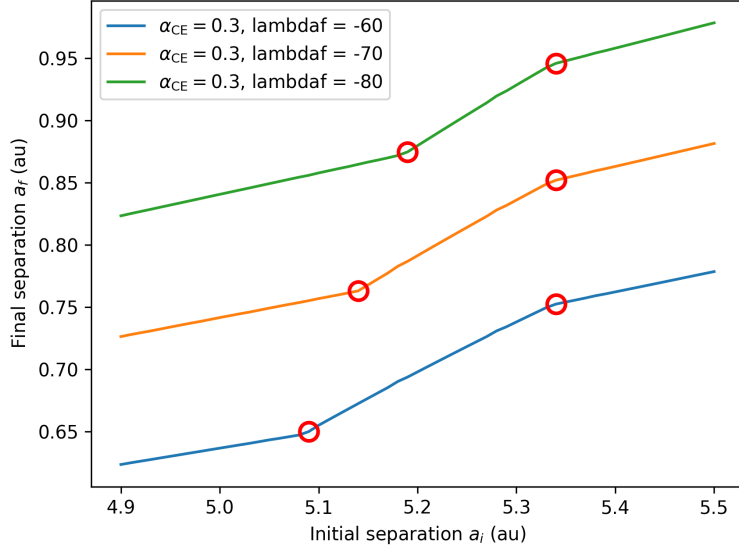


Figure 3: Dependence of final separation a_f on initial separation a_i for $\alpha_{CE} = 0.3$. Simulation results of $\lambda_f = 60, 70$, and 80 are shown. The red circles emphasize the jump of final separation as initial separation increases.

be clearly seen from the graph. After investigating the `bpp` array of these simulations, we find out the jump at about 2.9 au and 7.1 au is likely due to the difference of `kstar_1` at the start of RLOF. For $a_i < 2.9$ au, RLOF starts when `kstar_1 = 3` (First Giant Branch, GB). For $a_i = 2.9$ au, RLOF starts when `kstar_1 = 4` (Core Helium Burning, CHeB). For $2.9 \text{ au} < a_i < 7.1$ au, RLOF starts when `kstar_1 = 5`, (Early AGB, E-AGB). For $a_i > 7.1$ au, RLOF starts when `kstar_1 = 6`, (thermal-pulse AGB, TP-AGB).

Inspecting more closely, we find that the final separation a_f jumps at about $5.2 \sim 5.4$ au. This is especially obvious with $\alpha_{CE} = 0.3$. To illustrate, we zoom in the simulation results of $\alpha_{CE} = 0.3$, and present the change of final separation a_f as initial separation a_i increases in Figure 3. From here, we can clearly see two jumps — one between 5.1 au and 5.2 au, the other at 5.34 au. To explain this, we again go to the `bpp` array of these systems. We notice that the first jump is probably because the evolution process changes from **3-7-8-4-3-7-8-4** to **3-7-8-7-8-4**. This means that for relatively larger initial separation a_i , the primary fills its Roche lobe all the time, leading to more mass loss during a shorter timescale and thus larger final separation. Also, the second jump is probably because `kstar_1` changes from 8 (Naked Helium Star Hertzsprung Gap) to 9 (Naked Helium Star Giant Branch) at the start of the second common envelope. This changes the binding energy of the common envelope and thus changes the final separation.

Finally, notice that a small triangular gap in the figure for $\alpha_{CE} = 1$. This is because `kstar_1` becomes a neutron star and no rows in the `bpp` gets selected.

In conclusion, with a large `lambda_dof`, it is possible to create wide post-mass transfer WD+MS systems with final separation $a_f > 0.15$ au, which is the minimal separation of our observed objects.

2.1.3 Comparison

After we have obtained the simulation results for different initial conditions, now we can calculate the effective λ that matches with results in [Yamaguchi et al., 2024a]. We use the following method to build

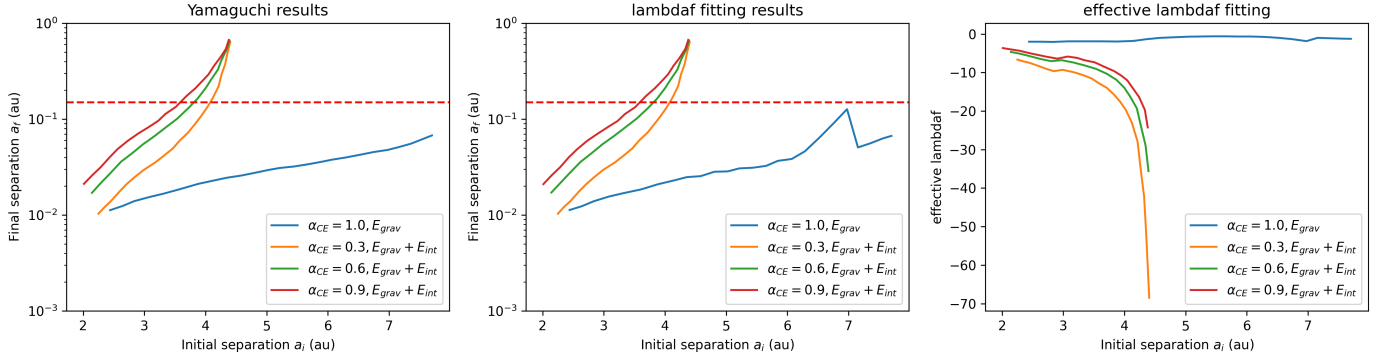


Figure 4: Effective λ fitting results of a $7M_\odot + 1M_\odot$ system for common envelope structure in MESA. *Left:* MESA results in [Yamaguchi et al., 2024a] of how final separation a_f depends on initial separation a_i . *Center:* COSMIC results of how final separation a_f depends on initial separation a_i , produced by the effective λ . *Right:* effective λ in COSMIC that corresponds to the MESA results for each initial separation a_i . The red line in the left and middle panel represents 0.15 au, the minimal separation for observed wide post-CE WD+MS binaries.

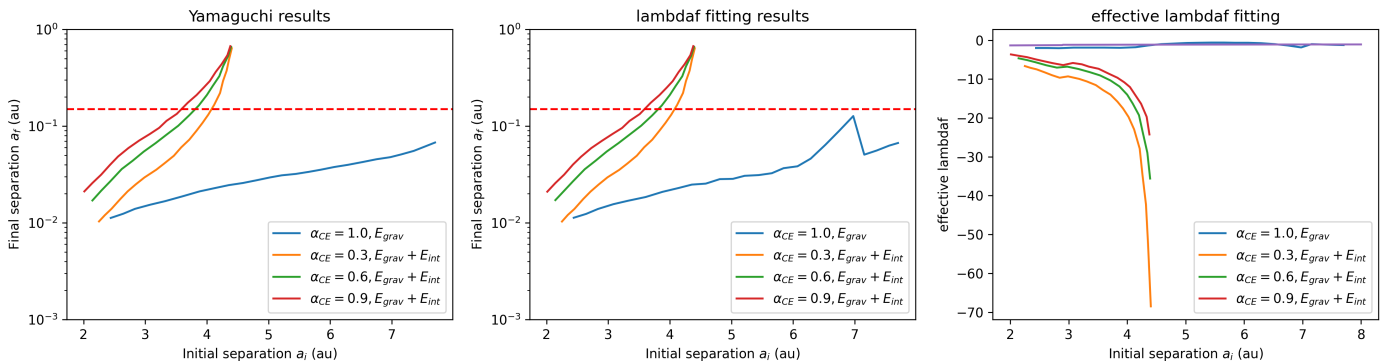


Figure 5: Same as Figure 4, but with default λ in COSMIC model included in the right panel.

the connection between COSMIC model and MESA model. For each fixed initial separation a_i , we loop through the COSMIC results with the same initial separation, and find the `lambdadaf` value that results in a final separation closest to MESA model results, documented in the figures of [Yamaguchi et al., 2024a]. We record this `lambdadaf` as the effective λ that matches the binding energy formalism at initial separation a_i .

For $E_{bind} = E_{grav} + E_{int}$, the fitting results is presented in Figure 4, where each line corresponds to different common envelope efficiencies α_{CE} and different energy budgets (either E_{grav} only or $E_{grav} + E_{int}$).

Notice that there is a small bump in the blue line. This is because at $6 \sim 7$ au, we cannot reach such low final separation in COSMIC while forming a WD+MS binary at the same time. In the left panel which shows the MESA results documented in [Yamaguchi et al., 2024a], we notice that even with low common envelope efficiencies, it is possible to create WD+MS binaries with final separation > 0.15 au in MESA as long as internal energy E_{int} is included. However, in the right panel we show that this correspond to very large `lambdadaf` in COSMIC ($\lambda > \sim 20$).

To further compare with the default λ value in COSMIC, we include in the right panel an extra line which represents the default λ value in COSMIC. This default λ in the COSMIC model is calculated following Appendix A of [Claeys et al., 2014]. For all of our case, we have $M_{env} > 1$. The results is shown in Figure 5. Notice that the default λ value is at order ~ 1 , far smaller than the effective λ needed to recreate results in [Yamaguchi et al., 2024a].

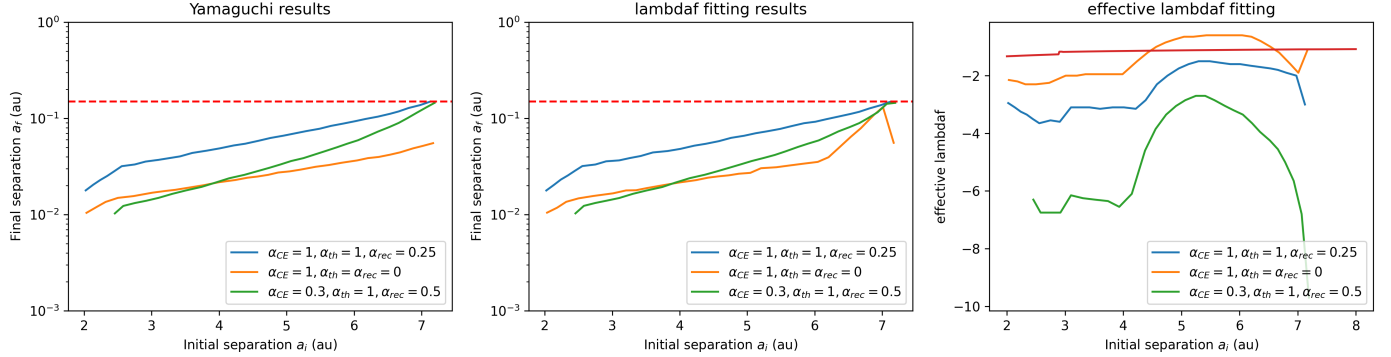


Figure 6: Same as Figure 5, but with a different energy budget.

For a different energy budge with $E_{\text{bind}} = E_{\text{grav}} + \alpha_{\text{th}}E_{\text{th}} + \alpha_{\text{rec}}E_{\text{rec}}$, the same results is shown in Figure 6

2.2 Low mass systems ($1.5M_{\odot} + 0.85M_{\odot}$)

In [Yamaguchi et al., 2024b], the author discussed the formation of WD+MS binaries through common envelope for low mass systems ($1.5M_{\odot} + 0.85M_{\odot}$). In this paper, the companion mass is set to be the median of observed systems $M_{\star} = 0.85M_{\odot}$, and the progenitor mass fot the WD is expected to be $1 \sim 3M_{\odot}$. Hence, $1M_{\odot}$, $1.5M_{\odot}$, and $3M_{\odot}$ models are run in MESA. For the energy budget, thermal energy E_{th} is fully included while the recombination energy E_{rec} is included in part with a parameter α_{rec} . That is,

$$E_{\text{bind}} = E_{\text{grav}} + E_{\text{th}} + \alpha_{\text{rec}}E_{\text{rec}}.$$

The results of MEsA models are shown in Figure 7

We take the same approach as in high mass systems to investigate the effective structural parameter λ that matches with the common evenlope model in MESA. We ran COSMIC binary evolution model for a system of $1.5M_{\odot} + 0.85M_{\odot}$ for different initial separation a_i and λ , to investigate how they affect the final separation a_f . The results in shown in Figure 8.

We compare this result with results in [Yamaguchi et al., 2024b] using the same appraoch as high mass systems. In the paper, the author presents separate results for two different method of calculating the binding energy. One of them contains binding energy of the entire envelope and the other only contains binding energy of the outer envelope. In Figure 9, we compare COSMIC with MESA model that includes binding enrgy of the entire envelope. In Figure 10, we compare with with MESA model that includes only binding energy of the outer envelope. Notice that we do not have fitting results for $a_i > 4$ au. This is because we do not get any WD+MS binaries in COSMIC for such initial separation range.

Based on the figure, we find that for low mass systems, the λ does not need to be far larger than default to produce WD+MS systems. This is a significant difference between high mass systems and low mass systems.

3 Stable Mass Transfer

After exploring the conditions of WD+MS binaries through common envelope, we investigate the possibility of WD+MS binaries formation through stable mass transfer. Similarly, we investigate the

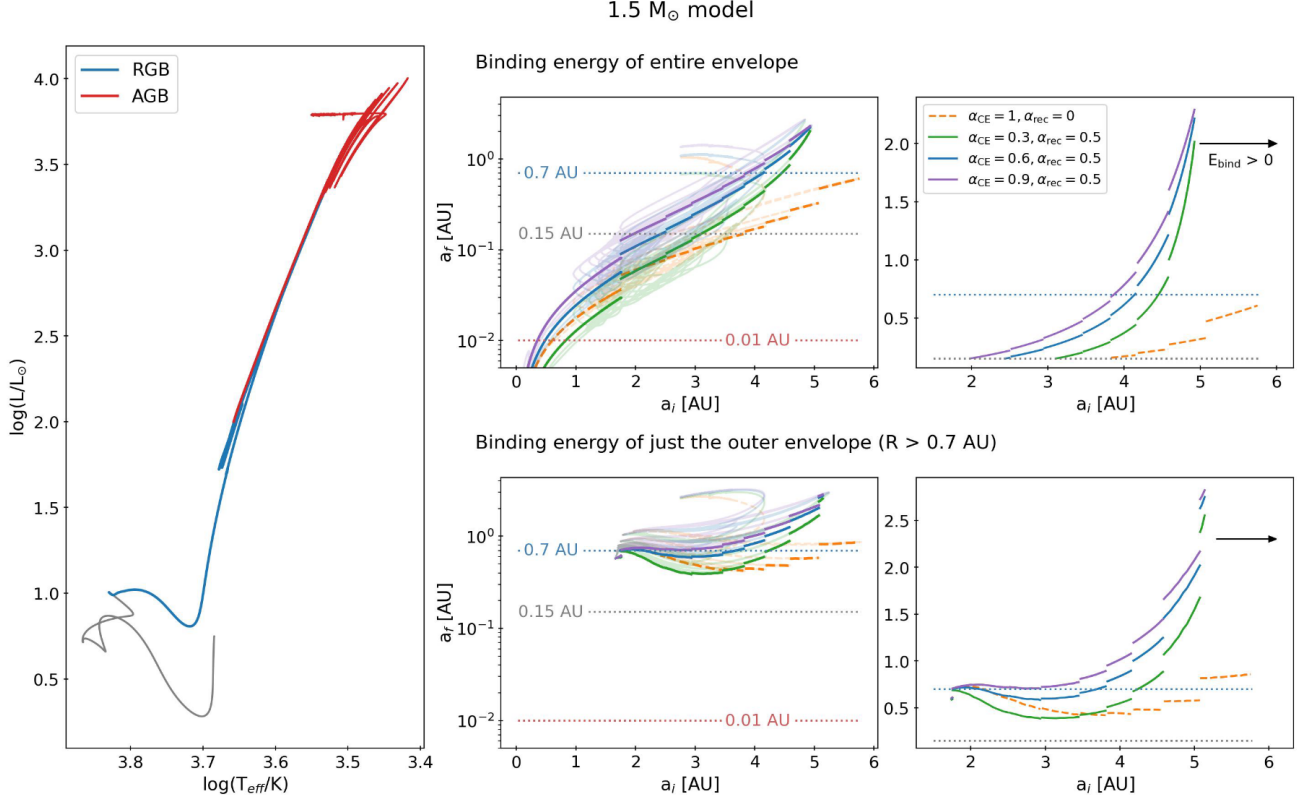


Figure 10. Same as Figure 9, but for a $1.5 M_{\odot}$ model. For this model, we see that wide orbits like those of our systems ($a_f > 0.7$ AU) do not form without recombination energy (orange dashed line) if the binding energy of the entire envelope is considered. Meanwhile, there is a small range of initial separations over which they can form if only the outer envelope is considered.

Figure 7: Results of how final separation a_f after common envelope depends on initial separation a_i for different common envelope efficiencies and energy budgets in [Yamaguchi et al., 2024b]. Here, for final separation $a_f < 0.01$ au, WD+MS binaries are not possible, while 0.15 au is the observed minimal separation and 0.7 au is the typical separation.

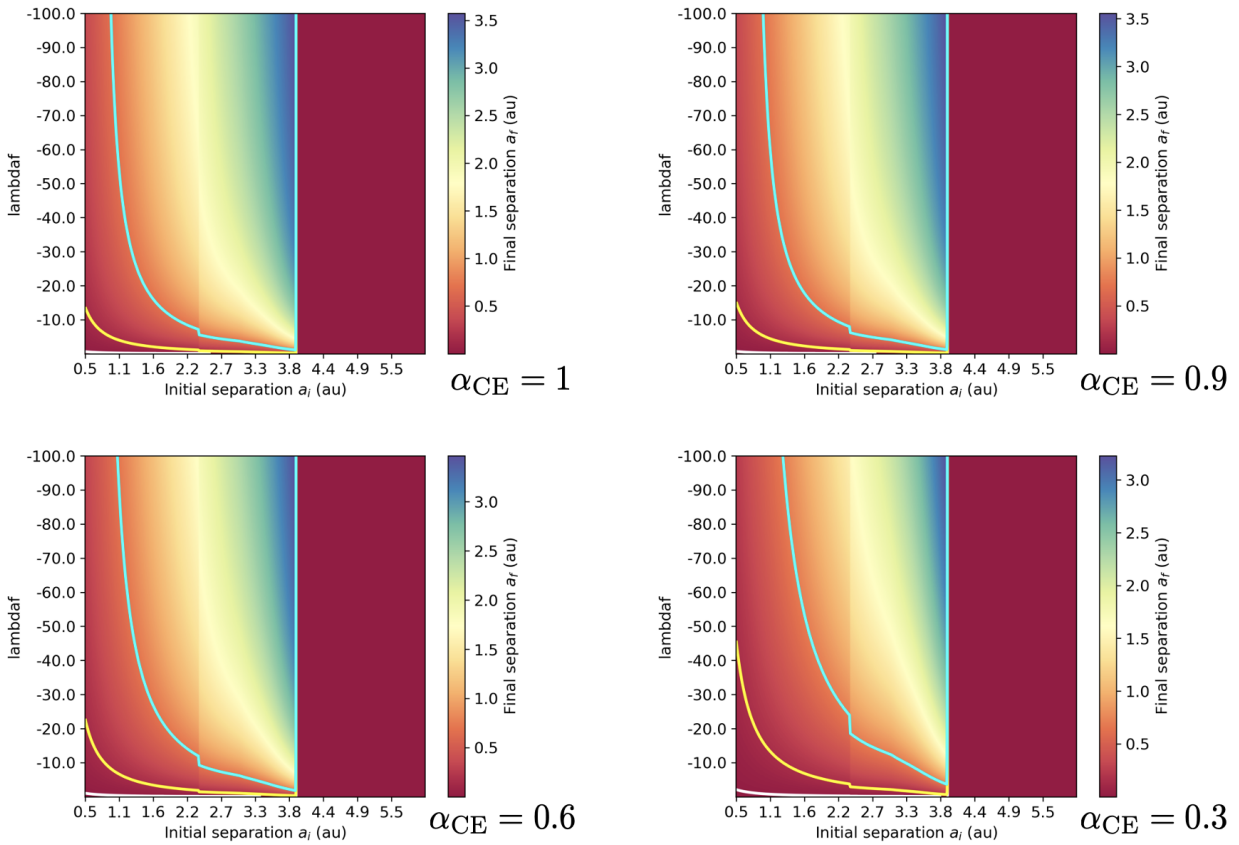


Figure 8: COSMIC results of how final separation a_f depends on initial separation a_i and common envelope flag "lambdaf" for different common envelope efficiencies α_{CE} , where the black and red contour corresponds to 0.01 au, 0.15 au, and 0.7 au as in Figure 7 respectively. Outside the black contour no desired system forms since WD+MS binaries are not possible for $a_f < 0.01$ au. 0.15 au and 0.7 au are the observed minimal separation and the typical separation respectively.

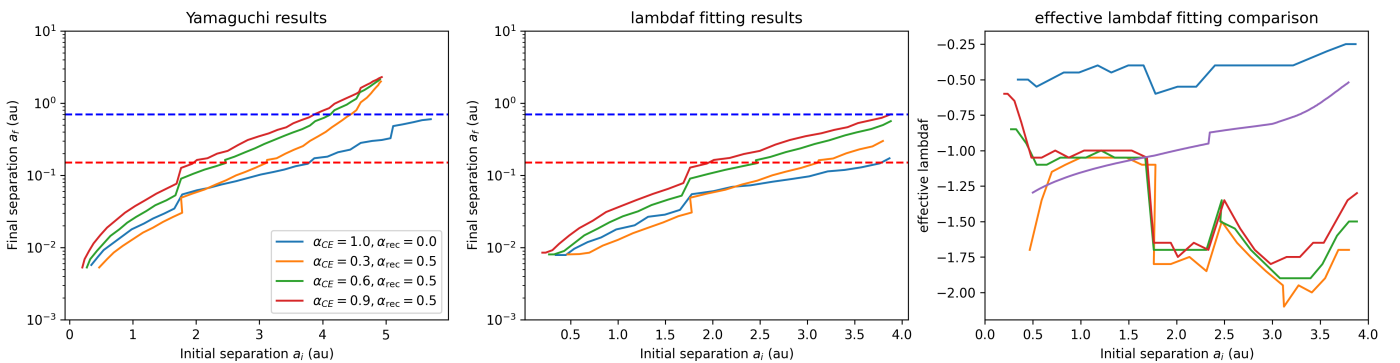


Figure 9: Effective λ fitting results of a $1.5M_\odot + 0.85M_\odot$ system for common envelope structure in MESA. Binding energy of the **entire envelope** is considered. *Left:* MESA results in [Yamaguchi et al., 2024b] of how final separation a_f depends on initial separation a_i . *Center:* COSMIC results of how final separation a_f depends on initial separation a_i , produced by the effective λ . *Right:* effective λ in COSMIC that corresponds to the MESA results for each initial separation a_i . The purple line represents default λ calculated using [Claeys et al., 2014]. The red line and the blue line in the left and middle panel represents 0.15 au and 0.7 au respectively. 0.15 au is the minimal separation for observed wide post-CE WD+MS binaries while 0.7 au is the typical separation for such systems.

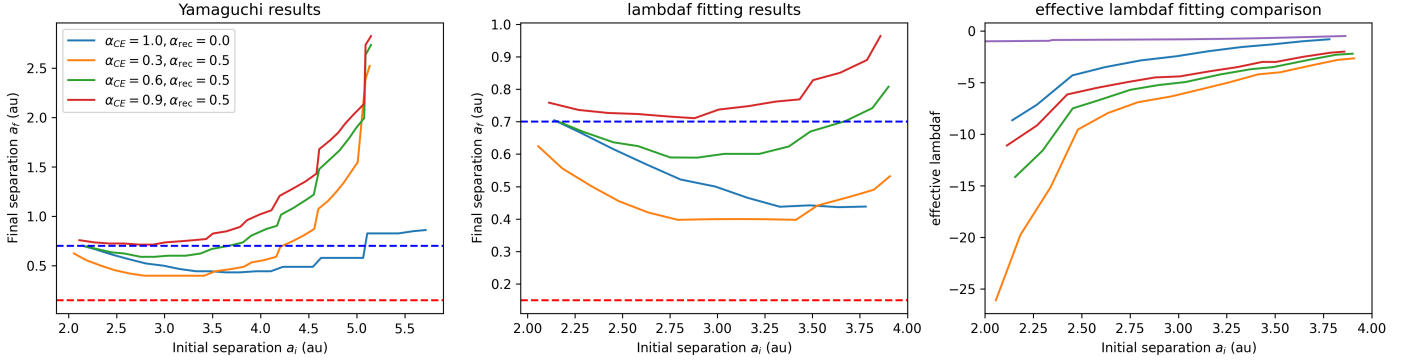


Figure 10: Same as Figure 10 but only binding energy of the **outer envelope** is included.

condition of forming both high mass systems ($7M_\odot + 1M_\odot$) and low mass systems ($1.5M_\odot + 0.85M_\odot$) through stable mass transfer.

3.1 High mass systems ($7M_\odot + 1M_\odot$)

3.1.1 Methods and results

First of all, to ensure stable mass transfer, we modify every entry of the `qcrit_array` in `BSEDict` from the default 0.0 to 20.0. This will make the actual mass ratio of our system below this critical value for common envelope throughout the entire process of mass transfer.

Secondly, to investigate dependence on different accretion efficiency, we modify the `acc_lim` flag in `BSEDict`, that is, the fraction β of all transferred materials is accreted by the accretor, or $\dot{M}_a = -\beta \dot{M}_d$. For each accretion efficiency, we run COSMIC binary simulation of a $7M_\odot + 1M_\odot$ system for initial separation ranging from 2 au to 8 au. After the simulation is finished, we select the first row, if any, that shows a WD+MS binary from `bpp` for each initial separation, and document the final separation. In this way, we can see how final separation depends on the initial separation, and we can compare them with the observed minimum separation 0.15 au.

The results are presented in Figure 11. The gap in the center means no WD+MS system forms for that initial separation. In fact, a closer inspection of the `bpp` shows that for these systems, two stars merge. The details of the `bpp` will be discussed in a more detailed manner in the next section.

Notice that the majority of these systems have final separation $a_f > 0.15$ au. However, this is **not the correct approach**, since the companion mass in our observed wide WD+MS binaries has median mass $\sim 1M_\odot$. However, in the simulation results shown in Figure 11, the final companion mass is about $4M_\odot$ and $6.5M_\odot$ for `acc_lim` = 0.5 and `acc_lim` = 1.0 respectively. Hence, we need to adjust the initial companion mass $M_{*,i}$ and the accretion efficiency `acc_lim`, in order to make the final companion mass $M_{*,f}$ close to $1M_\odot$.

Therefore, we lower the initial companion mass $M_{*,i}$ and adjust the accretion efficiency `acc_lim` and re-run the simulation. The results for $7M_\odot + 0.7M_\odot$ with `acc_lim`=0.1, and $7M_\odot + 0.5M_\odot$ with `acc_lim` = 0.2 is shown in Figure 12.

After adjusting the initial mass of companion and the accretion efficiency, now the final mass of the companion is about $1M_\odot$ and we get systems similar to our observed sample. Notice that when initial separation a_i is in the range of about 2.5 au to 4.5 au, the final separation increases rapidly. Also, it is only in this region that the final separation goes larger than the observed minimum 0.15 au. Hence, in the next subsection, we focus on this sharp increase and try to explain it qualitatively.

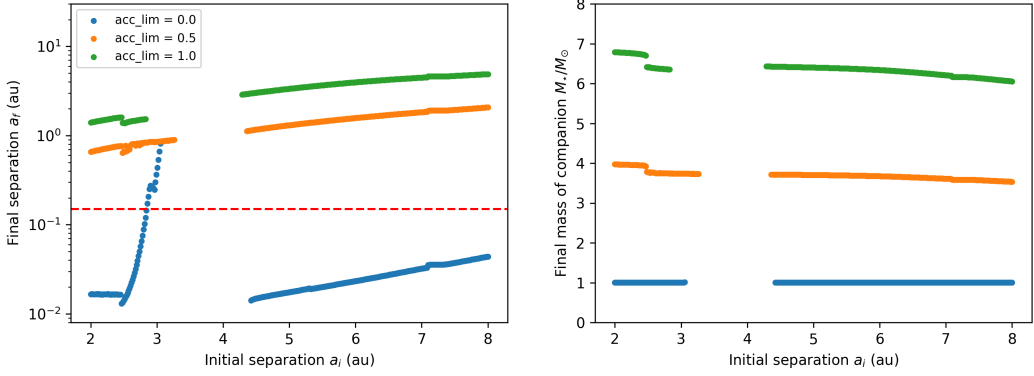


Figure 11: COSMIC results of WD+MS binaries after stable mass transfer for $7M_\odot + 1M_\odot$ systems, with accretion efficiency $\beta = 0$, $\beta = 0.5$, and $\beta = 1$ respectively. *Left:* dependence of final separation a_f of the WD+MS binary on initial separation a_i . *Right:* The corresponding companion mass in solar units in the WD+MS binary. The gap in both figure represents that no WD+MS system forms for that initial separation.

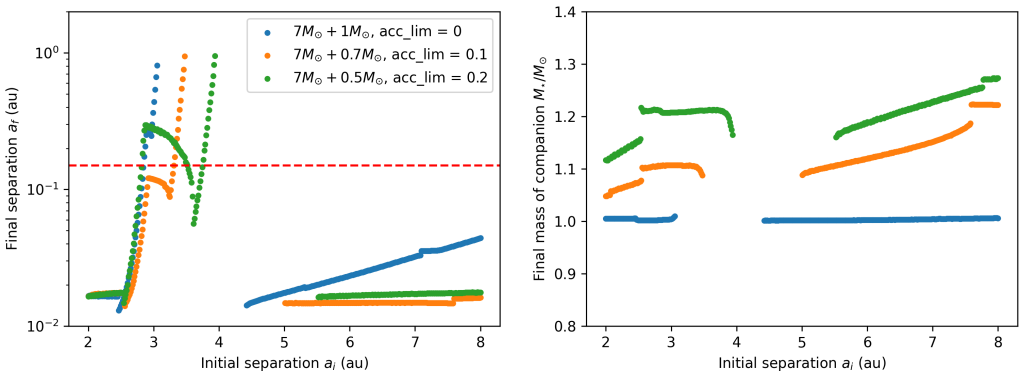


Figure 12: COSMIC results of WD+MS binaries after stable mass transfer for two systems — $7M_\odot + 0.7M_\odot$ with accretion efficiency $\beta = 0.1$, and $7M_\odot + 0.5M_\odot$ with accretion efficiency $\beta = 0.2$. The left and right panel presents the same content as in Figure 11.

bpp for $a_i = 2.30$ au — pre-spike

tphys	mass_1	mass_2	kstar_1	kstar_2	sep in AU	evol_type
0.000000	7.000000	1.000000	1.0	1.0	2.298116e+00	1.0
48.459967	6.944129	1.000000	2.0	1.0	2.314278e+00	2.0
48.617920	6.943478	1.000001	3.0	1.0	2.313945e+00	2.0
48.667633	6.942361	1.000009	3.0	1.0	1.710068e+00	3.0
48.678764	6.939198	1.000019	4.0	1.0	1.706148e+00	2.0
48.811288	2.915428	1.000138	4.0	1.0	1.404682e-02	5.0
48.811288	2.915428	1.000138	4.0	1.0	1.404682e-02	7.0
48.811288	1.351537	1.000138	7.0	1.0	1.340096e-02	8.0
48.811288	1.351537	1.000138	7.0	1.0	1.340096e-02	4.0
59.411358	1.307349	1.001526	8.0	1.0	1.326054e-02	2.0
60.284944	1.290687	1.002599	8.0	1.0	1.331702e-02	3.0
60.443051	0.835641	1.005400	8.0	1.0	1.655636e-02	4.0
60.446534	0.835371	1.005408	11.0	1.0	1.655861e-02	2.0
1918.791318	0.835371	1.005408	11.0	1.0	1.084571e-02	3.0
2211.771249	0.835371	0.743892	11.0	0.0	8.182929e-03	2.0
7951.247645	0.835371	0.084177	11.0	0.0	2.205755e-09	5.0
7951.247645	0.919547	0.000000	6.0	15.0	0.000000e+00	6.0
7951.534303	0.841397	0.000000	11.0	15.0	0.000000e+00	2.0
20000.000000	0.841397	0.000000	11.0	15.0	0.000000e+00	10.0

bpp for $a_i = 2.90$ au — spike

tphys	mass_1	mass_2	kstar_1	kstar_2	sep in AU	evol_type
0.000000	7.000000	1.000000	1.0	1.0	2.897624	1.0
48.459967	6.944129	1.000000	2.0	1.0	2.918003	2.0
48.617920	6.943478	1.000001	3.0	1.0	2.918316	2.0
48.678764	6.941467	1.000014	4.0	1.0	2.179365	2.0
48.678942	6.941448	1.000015	4.0	1.0	2.161114	3.0
48.680816	6.941297	1.000016	4.0	1.0	2.162553	4.0
54.850804	6.736319	1.001228	5.0	1.0	2.540353	2.0
54.911822	6.731331	1.001280	5.0	1.0	2.252056	3.0
55.052047	2.322664	1.001502	5.0	1.0	0.013314	5.0
55.052047	2.322664	1.001502	5.0	1.0	0.013314	7.0
55.052047	1.775220	1.001502	8.0	1.0	0.013181	8.0
55.052047	1.775220	1.001502	8.0	1.0	0.013181	4.0
55.052047	1.775220	1.001502	8.0	1.0	0.013181	3.0
55.052051	1.774498	1.001502	8.0	1.0	0.290706	4.0
55.063117	1.771428	1.001738	8.0	1.0	0.290866	3.0
55.082133	1.698036	1.002351	9.0	1.0	0.289273	2.0
55.101023	1.148543	1.003410	9.0	1.0	0.269165	4.0
55.103233	1.147894	1.003466	12.0	1.0	0.269198	2.0
12014.977421	1.147894	1.003466	12.0	2.0	0.269224	2.0
12647.908891	1.147902	1.002925	12.0	3.0	0.269253	2.0
13427.949122	1.149881	0.989522	12.0	3.0	0.259629	3.0
13460.125551	1.184615	0.348827	12.0	3.0	0.793729	4.0
13461.052193	1.185909	0.346316	12.0	10.0	0.792539	2.0
20000.000000	1.185909	0.346316	12.0	10.0	0.792547	10.0

Figure 13: COSMIC simulation data of $7M_{\odot} + 1M_{\odot}$ systems with accretion efficiency $\beta = 0$ and initial separation 2.30 au and 2.90 au respectively. They represent typical "pre-spike" binaries and "spike" binaries. The blue rectangle marks out the common first phase of evolution in both systems — contact and common envelope mass transfer.

3.1.2 Discussions

In the previous section, we mentioned how $7M_{\odot} + 1M_{\odot}$ systems with $\text{acc_lim} = 0$, $7M_{\odot} + 0.7M_{\odot}$ systems with $\text{acc_lim} = 0.1$, and $7M_{\odot} + 0.5M_{\odot}$ systems with $\text{acc_lim} = 0.2$ produces WD+MS binaries with final separation $a_f > 0.15$ au and companion mass $\sim 1M_{\odot}$ in certain range of initial separation a_i . From the figure, we can clearly see that when initial separation a_i is in the range of 2.5 au \sim 4.5 au, the final separation increases sharply as initial separation increases. In this section, we investigate the reason behind this by focusing on $7M_{\odot} + 1M_{\odot}$ binaries with $\text{acc_lim} = 0$.

First of all, let's take a look at how the final separation a_f depends on the initial separation a_i throughout the range of 2 \sim 8 au. In general, as shown in Figure 12, the dependence of a_f on a_i can be roughly divided into four parts — **pre-spike**, **spike**, **merge**, and **after-merge**, which corresponds to the part before the sharp increase ($a_i < 2.5$ au), the part where final separation increases sharply (2.5 au $<$ $a_i < 3.5$ au), the part where the binary merges and no desired system is formed (3.5 au $<$ $a_i < 4.5$ au), and the part after that ($a_i > 4.5$ au).

A typical **pre-spike** bpp is presented in the left panel of Figure 13. Notice that the binary come into contact ($\text{evol_type} = 5$), which follows by a common envelope phase. The same is observed in **spike** binaries, as shown in the right panel of 13.

Two typical **spike** bpp is presented in Figure 14. In the left panel, we notice that the stable mass transfer process in the green rectangle widens the orbit a lot. In the right panel, the extra stable mass transfer process in the red rectangle also significantly widens the orbit. However, in the right panel, the orbit widens without the primary's losing a lot of mass, and the corresponding mass transfer in green does not widen the orbit, even shrinking it.

To qualitatively explain thses results, note first that for a stable and non-conservative and the mass, we have

$$\frac{j}{J} \propto (1 - \beta) q_d \frac{\dot{M}_d}{M_T}.$$

While $a \sim J^2$, the non-conservative mass transfer should causes the orbit to expand. Note also that mass

bpp for $a_i = 2.80$ au — spike

tphys	mass 1	mass 2	kstar 1	kstar 2	sep in AU	evol type
0.000000	7.000000	1.000000	1.0	1.0	2.797706	1.0
48.459967	6.944129	1.000000	2.0	1.0	2.817382	2.0
48.617920	6.943478	1.000001	3.0	1.0	2.817668	2.0
48.677334	6.941615	1.000014	3.0	1.0	2.089388	3.0
48.678764	6.941468	1.000015	4.0	1.0	2.009718	2.0
48.776277	6.931278	1.000131	4.0	1.0	2.089573	4.0
54.850804	6.736677	1.001288	5.0	1.0	2.381054	2.0
54.895918	6.733153	1.001326	5.0	1.0	2.170262	3.0
55.040413	2.369074	1.001534	5.0	1.0	0.013292	5.0
55.040413	2.369074	1.001534	5.0	1.0	0.013292	7.0
55.040413	1.775220	1.001534	8.0	1.0	0.013148	8.0
55.040413	1.775220	1.001534	8.0	1.0	0.013148	4.0
55.040413	1.775220	1.001534	8.0	1.0	0.013148	3.0
55.059883	1.585227	1.002053	9.0	1.0	0.093256	2.0
55.064839	1.093955	1.002279	9.0	1.0	0.090912	4.0
55.067346	1.093432	1.002343	12.0	1.0	0.090914	2.0
12066.990212	1.093432	1.002343	12.0	2.0	0.090829	2.0
12702.675854	1.093466	1.001802	12.0	3.0	0.090596	2.0
13332.549577	1.093901	0.999140	12.0	3.0	0.085036	3.0
13490.812845	1.116272	0.277346	12.0	3.0	0.384219	4.0
13495.257742	1.117555	0.275304	12.0	10.0	0.383536	2.0
20000.000000	1.117555	0.275304	12.0	10.0	0.383536	10.0

bpp for $a_i = 2.90$ au — spike

tphys	mass 1	mass 2	kstar 1	kstar 2	sep in AU	evol type
0.000000	7.000000	1.000000	1.0	1.0	2.897624	1.0
48.459967	6.944129	1.000000	2.0	1.0	2.918003	2.0
48.617920	6.943478	1.000001	3.0	1.0	2.918316	2.0
48.678764	6.941467	1.000014	4.0	1.0	2.179365	2.0
48.678942	6.941448	1.000015	4.0	1.0	2.161114	3.0
48.680316	6.941297	1.000016	4.0	1.0	2.162553	4.0
54.850804	6.736319	1.001228	5.0	1.0	2.540353	2.0
54.911822	6.731331	1.001280	5.0	1.0	2.252056	3.0
55.052047	2.322664	1.001502	5.0	1.0	0.013314	5.0
55.052047	2.322664	1.001502	5.0	1.0	0.013314	7.0
55.052047	1.775220	1.001502	8.0	1.0	0.013181	8.0
55.052047	1.775220	1.001502	8.0	1.0	0.013181	4.0
55.052047	1.775220	1.001502	8.0	1.0	0.013181	3.0
55.052051	1.774498	1.001502	8.0	1.0	0.290706	4.0
55.063117	1.771428	1.001738	8.0	1.0	0.290866	3.0
55.082133	1.698036	1.002351	9.0	1.0	0.289273	2.0
55.101023	1.148543	1.003410	9.0	1.0	0.269165	4.0
55.103233	1.147894	1.003466	12.0	1.0	0.269198	2.0
12014.977421	1.147894	1.003466	12.0	2.0	0.269224	2.0
12647.908891	1.147902	1.002925	12.0	3.0	0.269253	2.0
13427.949122	1.149881	0.989522	12.0	3.0	0.259629	3.0
13460.125551	1.184615	0.348827	12.0	3.0	0.793729	4.0
13461.052193	1.185909	0.346316	12.0	10.0	0.792539	2.0
20000.000000	1.185909	0.346316	12.0	10.0	0.792547	10.0

Figure 14: COSMIC simulation of systems $7M_{\odot} + 1M_{\odot}$ with accretion efficiency $\beta = 0$ and initial separation 2.80 au and 2.90 au respectively. The red rectangle emphasizes the extra mass transfer process that significantly widens the orbit without the primary losing significant mass.

transfer begins when the primary is a Naked Helium Star on the Hertzsprung Gap (`evol_type` = 8), whose wind mass loss is significant. Also, for wind mass loss, we have

$$\frac{\dot{a}}{a} = -\frac{\dot{M}}{M_T}.$$

Therefore, strong wind stripping mass from the primary will cause the orbit to expand even further. To illustrate this more clearly, we change the `windflag` in `BSEDict` to 0, which correspond to weak wind. Now the $a_i = 2.80$ au system has final separation $a_f = 0.05$ au, and the $a_i = 2.90$ au system has final separation $a_f = 0.14$ au, both smaller than the original 0.09 au and 0.27 au that correspond to stronger wind.

From the equations, it is not difficult to see that the increase of separation is more obvious for larger separation a for both wind mass loss and stable, non-conservative mass transfer. Therefore, we conclude qualitatively that for **pre-spike** and **spike** systems, non-conservative mass transfer and wind mass loss widens the orbit. While this is more obvious for large separation a , this accounts for the spike of final separation a_f as the initial separation a increases.

A typical **merge** and an **after-merge** system are presented in Figure 15. Notice that for the merge systems, the two stars come in contact and a common envelope process follows, similar to **spike** systems. Compared to the **spike** systems, we notice that the separation of the binary at the start of the common envelope is smaller in **merge** systems than in **spike** systems. This qualitatively explains the reason for the merging — the orbit does not have enough energy to eject the common envelope and two star merges. In contrast, the **after-merge** systems possesses more energy than the **merge** systems due to their larger initial separation. Hence, they either survives the common envelope or do not come into contact at all. This explains why desired WD+MS systems form again as the initial separation a_i increases.

This concludes our qualitative analysis on the evolution results of $7M_{\odot} + 1M_{\odot}$ through stable mass transfer. Again, as shown in Figure 11, for stable mass transfer, the observed minimum separation of wide post-mass transfer WD+MS systems 0.15 au can only be achieved in the **spike** region. That is, in

bpp for $a_i = 3.25$ au — merge

tphys	mass_1	mass_2	kstar_1	kstar_2	sep in AU	evol_type
0.000000	7.000000	1.000000	1.0	1.0	3.247337	1.0
48.459967	6.944129	1.000000	2.0	1.0	3.270176	2.0
48.617920	6.943478	1.000001	3.0	1.0	3.270527	2.0
48.678764	6.941467	1.000012	4.0	1.0	2.920264	2.0
54.850804	6.736176	1.001964	5.0	1.0	2.923984	2.0
54.950802	6.726946	1.001154	5.0	1.0	2.476527	3.0
55.079899	2.349232	1.001419	5.0	1.0	0.011769	5.0
55.079899	2.349232	1.001419	5.0	1.0	0.011769	7.0
55.079899	3.350651	1.001419	5.0	15.0	0.000000	8.0
55.145276	1.775220	0.000000	9.0	15.0	0.000000	2.0
55.207957	1.694856	0.000000	9.0	15.0	0.000000	15.0
55.207957	1.260782	0.000000	13.0	15.0	0.000000	2.0
20000.000000	1.260782	0.000000	13.0	15.0	0.000000	10.0

bpp for $a_i = 5.00$ au — after-merge

tphys	mass_1	mass_2	kstar_1	kstar_2	sep in AU	evol_type
0.000000	7.000000	1.000000	1.0	1.0	4.995904e+00	1.0
48.459967	6.944129	1.000000	2.0	1.0	5.031040e+00	2.0
48.617920	6.943478	1.000000	3.0	1.0	5.031468e+00	2.0
48.678764	6.941467	1.000007	4.0	1.0	5.018299e+00	2.0
54.850810	6.735544	1.000569	5.0	1.0	5.099778e+00	2.0
55.083797	6.697128	1.000870	5.0	1.0	3.860463e+00	3.0
55.150278	6.599484	1.001293	6.0	1.0	3.558691e+00	2.0
55.176817	1.239417	1.001565	6.0	1.0	1.608474e-02	4.0
55.358820	1.238056	1.001777	12.0	1.0	1.606912e-02	2.0
1327.950277	1.238056	1.001777	12.0	1.0	1.169005e-02	3.0
1923.450468	1.238056	0.742584	12.0	0.0	9.115471e-03	2.0
6460.980514	1.238056	0.095052	12.0	0.0	1.141788e-09	5.0
6460.980514	1.333108	0.000000	6.0	15.0	0.000000e+00	6.0
6461.120196	1.243764	0.000000	12.0	15.0	0.000000e+00	2.0
20000.000000	1.243764	0.000000	12.0	15.0	0.000000e+00	10.0

Figure 15: COSMIC simulation of systems $7M_{\odot} + 1M_{\odot}$ with accretion efficiency $\beta = 0$ and initial separation 3.25 au and 5.00 au respectively. The blue rectangle emphasizes the differences of two evolution process, which also represents the typical difference between **merge** and **after-merge** systems.

our results, all wide post-mass transfer systems are due to the strong wind mass loss from the primary that widens the orbit significantly.

Similarly, in [Yamaguchi et al., 2024b], the author listed several arguments against the formation of wide post-mass transfer binaries through stable mass transfer. As shown in Figure 16, the observed wide post-mass transfer WD+MS binaries do not match the theoretical $M_{WD} - P_{orb}$ relation calculated in [Rappaport et al., 1995], where the grey region is set to be a factor of 2.5 away from the calculated line.

4 Population Simulation

After investigating how the final separation depends on various parameters in individual binary star systems, we now shift our focus onto the distribution of final orbital period in a population of binaries (or equivalently final separation since $P_{orb}^2 \sim a^3$).

4.1 Methods

First of all, we sample the binary population using the independent sampler in COSMIC. We set the primary mass model to `korupa01`, eccentricity model to `uniform`, and orbital period model, together with the binary fraction model to `moe19`. We sample a total number of about 10000 binaries with solar metallicity. The distribution of primary mass and the orbital period in the sampled population is shown in the Figure 17.

Now to investigate how the final white dwarf mass and orbital period depends on `lambdaf`, we simulation the sampled population with five different `lambdaf` values, -5 , -15 , -25 , -35 , and -45 , which corresponds to $\lambda = 5, 15, 25, 35$ and 45 in Equation 1. After that, for each binary star system in the population, we select the moment when CE is finished and when the system is a WD+MS one to record the white dwarf mass M_{WD} and final orbital period $P_{orb,f}$. We also select the moment when the first RLOF started to record the initial orbital separation $P_{orb,i}$. This will later on help us compare the difference and how much the orbit widens.

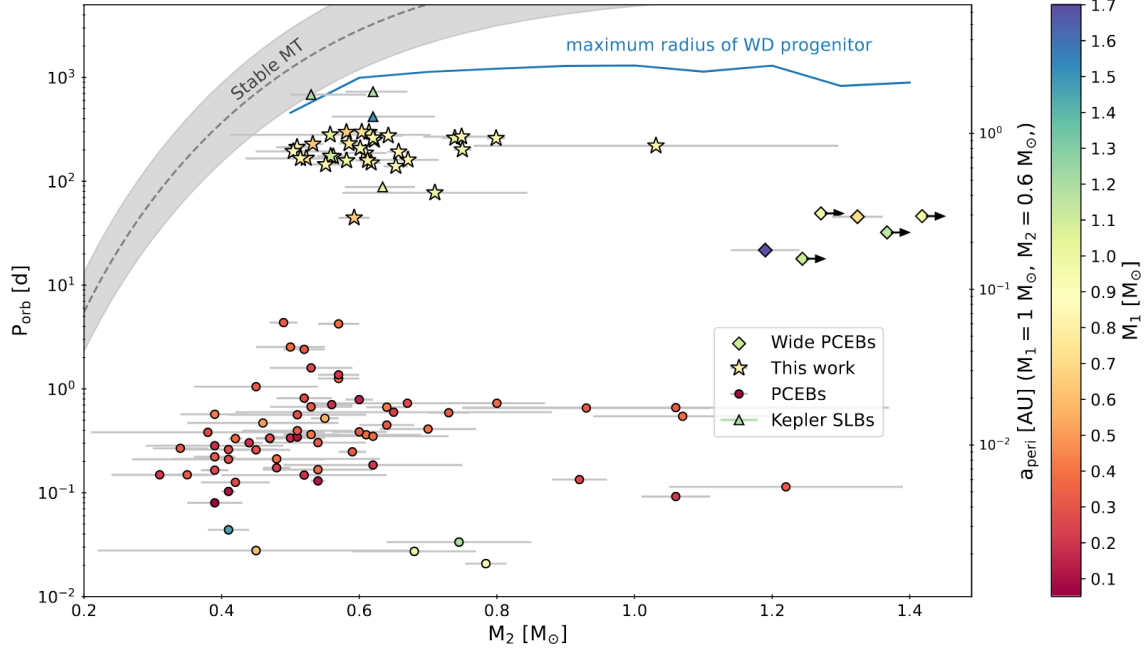


Figure 7. Orbital period, P_{orb} , against WD mass, M_2 . The colors of the points represent the masses of the luminous companion, M_1 . On the right axis, we show the minimum orbital separation, a_{peri} , corresponding to the period assuming $M_1 = 1 M_\odot$ and $M_2 = 0.6 M_\odot$. We plot the “short-period PCEBs” discovered with SDSS by Rebassa-Mansergas et al. (2007) as well as those from Hernandez et al. (2021, 2022a,b) with circle markers. “Wide PCEBs” which include IK Peg Wonnacott et al. (1993) and the systems from Yamaguchi et al. (2024b) are plotted with diamond markers. We also plot the self-lensing systems discovered with Kepler (Kruse & Agol 2014; Kawahara et al. 2018) with triangle markers. The solid line marks the maximum mass that is reached by the giant progenitor at each WD mass. The dashed line is the track along which binaries undergoing stable MT are expected to evolve Rappaport et al. (1995).

Figure 16: $M_{\text{WD}} - P_{\text{orb}}$ relation of observed wide post-mass transfer binaries. Binaries going through stable mass transfer is expected to fall in the grey region, as calculated in [Rappaport et al., 1995].

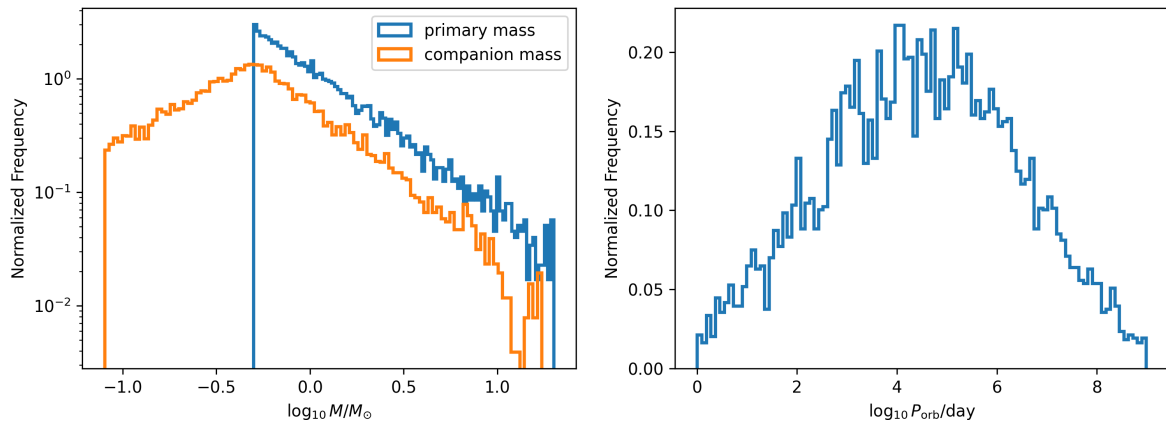


Figure 17: The distribution of primary mass, companion mass, and orbital period in the sampled population using independent sampler. *Left:* Distribution of primary mass and companion mass in log scale. *Right:* Distribution of orbital period P_{orb} in log scale.

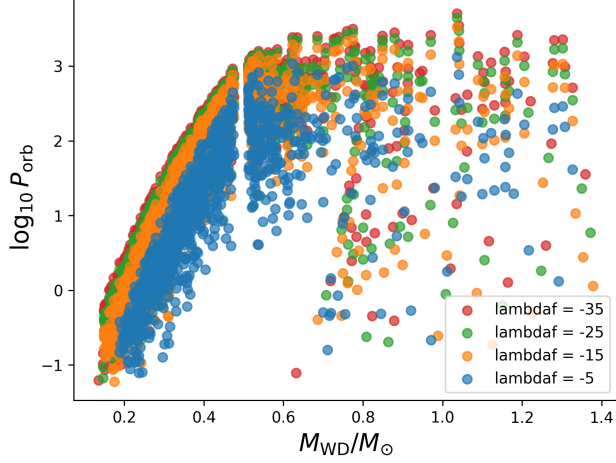


Figure 18: Scatter plot of white dwarf mass M_{WD} and final orbital period after common envelope in log scale $\log_{10} P_{\text{orb}}$. Different colors indicates results for different λ values. For each different λ value the same initial population is used.

4.2 Results

To show how the change in λ affects the final orbital period, a scatter plot presenting the correlation of final orbital period P_{orb} and white dwarf mass M_{WD} is presented in Figure 18. We can see from the figure that when λ increases, the final orbital period also increases. This is obvious for low M_{WD} . This correlation is expected since for larger λ , less energy is required to unbind the common envelope.

To also show how the final orbital separation P_{orb} depends on the `kstar_1` type at the start of first RLOF, we plot final orbital period P_{orb} against white dwarf mass M_{WD} for each `lambdaf` separately, and use different color to distinguish between different `kstar_1` type at the start of mass transfer. The plot is shown in Figure 19. We can see that if the star is at later stages of evolution (`kstar` large) when mass transfer starts, then the resulting white dwarf mass M_{WD} and orbital period P_{orb} is also larger. Notice that few systems start the mass transfer at `kstar_1` = 2 (Hertzsprung Gap) and `kstar_1` = 4 (Core Helium Burning). This is because stars crosses Hertzsprung gap in a short timescale, leaving little time for interaction. Also, stellar radius is small when going through Core Helium Burning, reducing the possibility of interactions that starts when `kstar_1` = 4.

To visualize the difference in final orbital period P_{orb} , and how they corresponds to different `kstar_1` type at the start of RLOF, we create scatter plot in Figure 20 of the difference in orbital period $\Delta P = P_{\text{orb}}^{\lambda=35} - P_{\text{orb}}^{\lambda=5}$ against the white dwarf mass M_{WD} .

From Figure 20, we can see that for large `kstar_1` type at the start of RLOF, $\Delta P = P_{\text{orb}}^{\lambda=35} - P_{\text{orb}}^{\lambda=5}$ is also larger. To explain this, we plot the how final white dwarf mass M_{WD} , difference in final orbital period ΔP_{orb} , and orbital period before mass transfer $P_{\text{orb},i}$ related to each other in Figure 21. We see that the larger initial orbital period $P_{\text{orb},i}$, the more significant effect does λ have on the final orbital period. This is not unexpected since during mass transfer, the separation changes as $a/a = \text{const}$. Hence $P_{\text{orb}}/P_{\text{orb}} = \text{const}$. Therefore, the larger the initial orbital period, the larger it changes, and thus the larger effect does λ have.

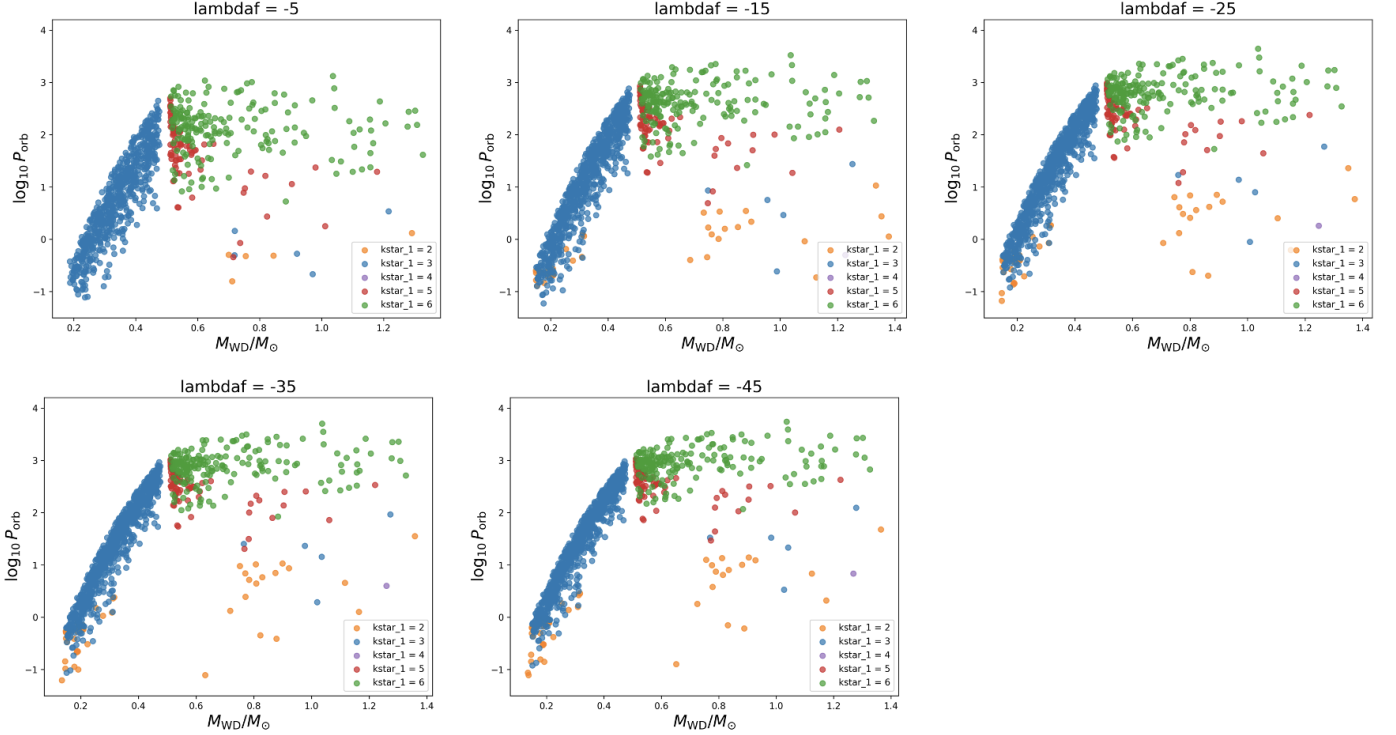


Figure 19: Each panel: for this λ value, scatter plot of white dwarf mass M_{WD} and final orbital period after common envelope in log scale $\log_{10} P_{\text{orb}}$. Different colors represent different kstar type of the primary at the start of mass transfer.

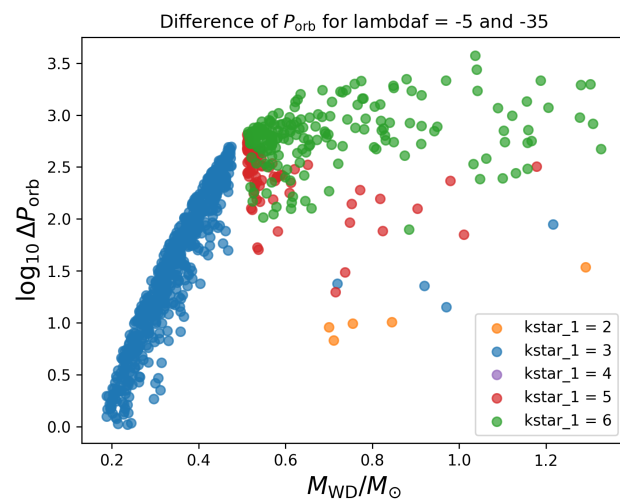


Figure 20: Scatter plot of difference in orbital period $\Delta P = P_{\text{orb}}^{\lambda=35} - P_{\text{orb}}^{\lambda=5}$ against the white dwarf mass M_{WD} . Different colors indicates different kstar type of the primary at the start of mass transfer.

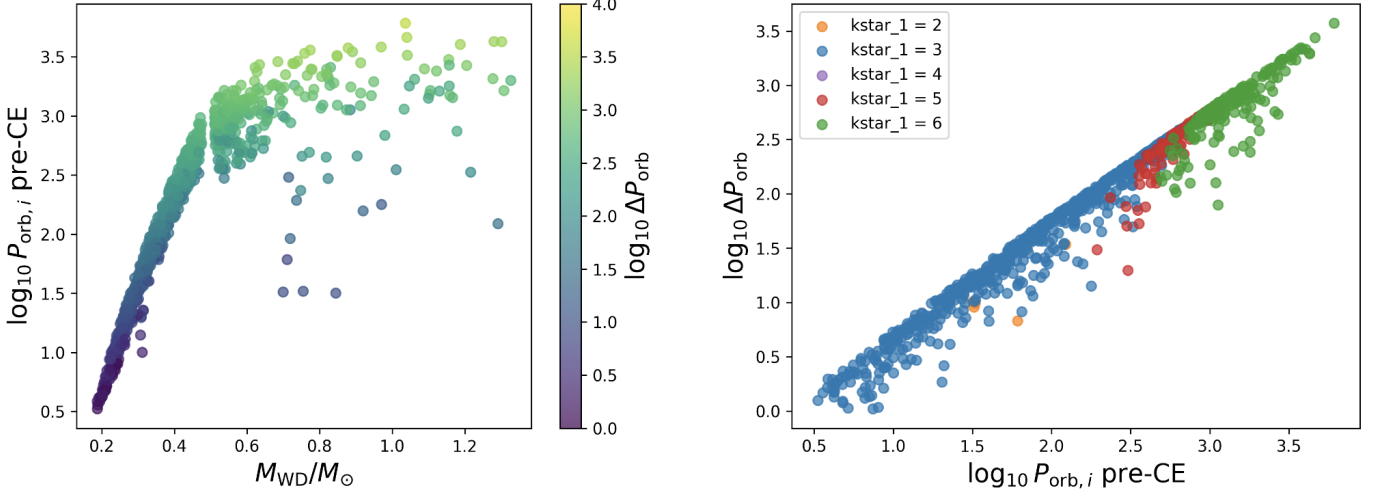


Figure 21: Left panel: scatter plot of initial orbital period at the start of RLOF $P_{\text{orb},i}$ against the final white dwarf mass M_{WD} . The color of the dots indicates how the final orbital period $P_{\text{orb},f}$ changes with respect to $\lambda = 35$ and $\lambda = 5$. That is, the color indicates the magnitude of $\Delta P = P_{\text{orb}}^{\lambda=35} - P_{\text{orb}}^{\lambda=5}$. Right panel: scatter plot of $\log_{10} \Delta P_{\text{orb}}$ against the initial orbital period in log scale $\log_{10} P_{\text{orb},i}$ at the start of RLOF. Different colors indicates different kstar type of the primary at the start of RLOF.

References

- [Claeys et al., 2014] Claeys, J., Pols, O., Izzard, R., Vink, J., and Verbunt, F. (2014). Theoretical uncertainties of the type ia supernova rate. *Astronomy & Astrophysics*, 563:A83.
- [Rappaport et al., 1995] Rappaport, S., Podsiadlowski, P., Joss, P., Di Stefano, R., and Han, Z. (1995). The relation between white dwarf mass and orbital period in wide binary radio pulsars. *Monthly Notices of the Royal Astronomical Society*, 273(3):731–741.
- [Yamaguchi et al., 2024a] Yamaguchi, N., El-Badry, K., Fuller, J., Latham, D. W., Cargile, P. A., Mazeh, T., Shahaf, S., Bieryla, A., Buchhave, L. A., and Hobson, M. (2024a). Wide post-common envelope binaries containing ultramassive white dwarfs: evidence for efficient envelope ejection in massive asymptotic giant branch stars. *Monthly Notices of the Royal Astronomical Society*, 527(4):11719–11739.
- [Yamaguchi et al., 2024b] Yamaguchi, N., El-Badry, K., Rees, N., Shahaf, S., Mazeh, T., and Andrae, R. (2024b). Wide post-common envelope binaries from gaia: orbit validation and formation models. *arXiv preprint arXiv:2405.06020*.